

Experimental Analysis of Friction Stir Welding of Dissimilar Aluminium Alloys by Machine Learning

Ambati Hemanth Sai Kumar, M.V.R. Durga Prasad, Yeole Shivraj Narayan*, Kode Jaya Prakash

¹ Department of Mechanical Engineering,

VNR Vignana Jyothi Institute of Engineering and Technology, Hyderabad, 500090, INDIA

*Corresponding Author: shivrajyeole@vnrvjiet.in

DOI: <https://doi.org/10.30880/ijie.2024.16.02.003>

Article Info

Received: 21 September 2023

Accepted: 15 October 2023

Available online: 15 April 2024

Keywords

Friction stir welding, analysis of variance (ANOVA), ultimate tensile strength, random forest regressor, artificial neural network

Abstract

Current research investigates friction stir welding of two disparate aluminium alloys - AA5083 and AA6082. Rotational speed of tool, its tilt angle & weld speed are optimized using L27 orthogonal design of experiments with tensile strength as the response. To assess plausible higher level machine learning approaches in anticipating friction stir welded AA5083 and AA6082 strength, random forest regressor and artificial neural network algorithms are employed. These models are used to investigate discrepancies between experimental and predicted results. Of the available results, 21 readings are chosen to train the model whereas remaining are utilized to test the model. Random forest regressor and artificial neural network techniques were formed using the data associated with the experiment. Moreover, results of the analysis of variances are compared to the machine learning predicted results to determine the variances.

1. Introduction

Alloys made from aluminium are recognized for their inherent and flexible properties, including corrosion prevention, formability, mechanical strength, low density, electrical conductivity, and low density. Due to these properties, it is highly sought after in a diverse variety of manufacturing sectors, construction of ships, packaging, automobiles, and architecture. Welding of aluminium alloys requires specialized expertise and experience as its demand is growing in many applications. Loss of strength is due to porosity, element loss, solidification, stress corrosion cracking's and incompatibilities among the workpiece and filler alloy in welding with dissimilar metals. This is when aluminium alloys are welded [1]. These issues can be addressed best by solid-state welding of aluminium alloys [2]. Efficient manufacturing and low energy usage have risen to the top of the prioritized government programs aimed at fostering long-term growth. Industries strive to adopt solutions that utilize the fewest resources, optimize manufacturing methods, and produce improved materials in an attempt to achieve economic and environmental sustainability. Because of the need to use as few resources as possible, manufacturing designs are trending toward complicated structural joints and joints using both the same metal and distinct metals [3]. Joining two dissimilar materials results in a fusion of material properties from both materials, making the joined weldments suitable for military-based applications such as lighter weight tanks, military bridges, battle tanks, body armor ambulances, titanium lightweight howitzers, layer tanks, and so on. Aluminium alloys are primarily used in fusion-based welding processes. However, fusion-based welding creates significant challenges due to changes in alloy composition, thermal characteristics, and other metallurgical and mechanical properties. Furthermore, weld solidification complications such as fractures, undercut, porosity, and so on reduce weldment quality, resulting in the occurrence of very coarse grains and intermetallic compounds at

the weld region and a drop in mechanical qualities. In addition to excellent mechanical properties, aluminium-magnesium alloys are also corrosion-resistant, workable, and weldable. AA EN AW5083 is one of the strongest Al-Mg alloys. Al-Mg-Si alloy is used to lighten the mass of vehicle components, especially body sheets with good corrosion resistance and medium strength. Despite its excellent weldability, EN AW6082 alloy has a reduced strength in the weld zone [2]. FSW tool does keep the base material unfused as illustrated in Fig. 1 [4].

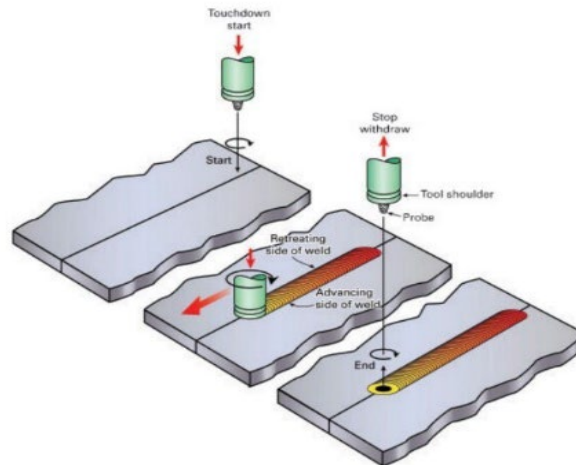


Fig. 1 FSW process [4]

Recent developments in the FSW process have incorporated machine-learning techniques. Welding-related challenges can be effectively addressed with machine learning. Welding and quality control can both be enhanced with the technology. As a result, defects can be detected in real-time during welding. Machine learning has been used to solve traditional welding process problems. A significant advantage of ML over simulation is that it significantly reduces the number of repetitive operations and the amount of time and money spent on data analysis. To distinguish between good and bad welds, we used the MSER method to extract images of the weld surfaces. It is 95.8% more accurate to identify good welds with a trained SVM model [5]. A sensitivity analysis indicates that rotational speed matters most. The RFM, M5P, and ANN models predict UTS levels accurately based on ANOVA analysis of the data set. The RFM technique outperforms the M5P tree and ANN [6]. In comparison to SVM and MLR regression techniques, RBF kernel-based GPR regression shows good performance [7]. RFM showed the highest coefficient of determination (0.926) compared with the other algorithms, indicating that the predictions are remarkably close to the experimental results [8]. ANN algorithms generate higher and more accurate results than Decision Tree regression techniques, according to this study. Increasing the number of data sets may improve the accuracy of both systems [9]. The UTS increases as the TRS and axial load increase. In response to a reduction in WS, the UTS decreases. 1199 rpm rotational speed of tool, 30 mm/minute weld speed & 9.0 kN axial load were utilized in measurement of ultimate TS, YS and % elongation of joints [10]. ANNs were discovered to be the most commonly utilized artificial intelligence approach, with an accuracy rate of approximately 95%. For FSW Mechanical characteristics, the average error for ANN methods was around 5% [11]. The reliability and accuracy of ANN were found to be higher than RSM when compared with RSM. During training and test, SVM is capable of predicting results with over 100% accuracy. ANN methods have been eclipsed in popularity by SVM methods in machine learning [12]. The post-pruned best initial tree generated more precise results than a pre-pruned one at 1800 rpm. Relative to postpruned tree, the best initial tree generated the highest accuracy when 1400 rpm pre-pruning was applied. This may serve as a learning model during fusing AA in FSW [13]. During training, model was subjected to Levenberg-Marquardt. Prediction errors in artificial neural networks are relatively low. Correlation coefficients are 0.8214 in the model [14].

Compared to Ideal and Butterworth filters, the Gaussian filter produces smoother texture and less distortion [15]. Experimental studies optimizing Friction Stir Welding variables waste time and resources, increasing experiment costs. To overcome these difficulties, machine learning methods including ANN and image processing are applied [16]. The TRS ~ 1812 rpm, WS ~ 26 mm/min, and TTA ~ 1.3° are found to have the lowest values of UTS. Maximum UTS is attained at 1325 rpm TRS, 35 mm/min WS & 1.65° TTA. ANN exhibited best accuracy and LR least, following an examination of the accuracy of several regression models [17]. The experiment results show that the proposed Local Binary Pattern (LBP) algorithm saves money and time while outperforming the conventional staff inspection approach. It is worthwhile to investigate if LBP images that be used as an effective texture descriptor [18]. When the ANN is applied to the input dataset, the accuracy score is 0.95. The ANN algorithm has the maximum accuracy at 0.95, while the Random Forest and Decision Tree algorithms achieved least accuracy at 0.50. More datasets must be submitted for enhancing accuracy [19]. The 6.5 mm pin has a greater

UTS of 183 MPa, which is equivalent to a 75 percent joint efficiency, while the 2.5 mm pin has a minimum tensile strength of 42 MPa [20]. The weld rate has a substantial influence on ultimate strength and flawless joint, with 80 mm/min maximum speed achieving satisfactory tensile strength with a joint performance of 90% [21]. Minimum UTS of 113.5 MPa at 1200 rpm rotation speed, 90 mm/min WS, and 0° TTA was recorded [22].

Accordingly, prior research has examined characterization of joints under various methods. Machine learning approaches are mostly not examined in the literature for processing FS welded dissimilar AA 5083-AA6082. It is only in recent years that ANNs and SVMs have been used for predicting and validating experimental outcomes. This research aims to develop and validate ANN and RFR approaches for predicting the UTS of stir welded dissimilar materials AA5083-AA6082. Google Collaboratory (Colab) software is used to implement these machine learning approaches. Consequently, Taguchi's L27 OA is employed to conduct FSW experiments to determine the amount of data needed to train machine learning algorithms. Experimental curves are compared to determine how well the ANN and RFR predict. The test data is used to determine the most appropriate modelling technique. After that, the results of every ML approach are compared. As well as that, ANOVA is conducted with Minitab software to identify which parameter has the greatest effect and to compare it with ML feature importance analysis.

Nomenclature	
ANN	artificial neural network
FSW	friction stir welding
MAE	mean absolute error
ML	machine learning
MSE	mean squared error
OA	orthogonal array
RFR	random forest regressor
RMSE	root mean squared error
TRS	tool rotation speed
TTA	tool tilt angle
UTS	ultimate tensile strength
WS	welding speed
YS	yield strength

2. Friction Stir Welding

2.1 Materials and Methods

FSW welding was done on Aluminium alloys of 5xxx and 6xxx series of plates AA5083 and AA6082 with H13 tool material. Table 1 exhibits chemical configuration of AA5803 & AA6082. Utilizing a power hacksaw, the required plate specifications are 102 mm x 58 mm x 6.1 mm. The faying edges are then cut on a vertical milling machine to prevent faying edges imbalanced during the welding process. Fig. 2 shows the plate dimensions of AA5083 and AA6082 plates.

Table 1 Chemical configuration of AA alloys in weight %

Material	Al	Cu	Mg	Si	Mn	Fe	Zn	Ti	Cr
AA5083	94.687	0.049	4.09	0.14	0.47	0.38	0.031	0.031	0.15
AA6082	97.067	0.054	0.83	1.04	0.59	0.38	0.005	0.019	0.051

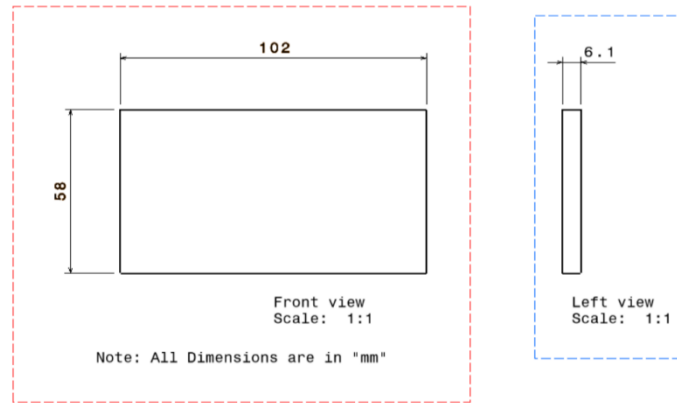


Fig. 2 Plate dimensions

In welding, a hexagonal pin profile tool shoulder manufactured from H13 with a 65 HRC hardness was used to create heat and stir the material. Fig. 3 represents the tool pin profile dimensions and the hexagonal tool pin manufactured from H13 material. To perform FSW operations, a universal milling machine needs to be converted to produce fixtures and tools. Based on literature research and machine tool capabilities, the control parameters TRS, WS and TTA were chosen for optimizing UTS response. Table 2 shows the process variables. Experimentally, the higher tensile strength material (AA5083) is clamped towards the advancing side of the universal milling machine in order superior tensile characteristics. Fig. 4 illustrates plate clamping in fixtures and the FSW joining operation.

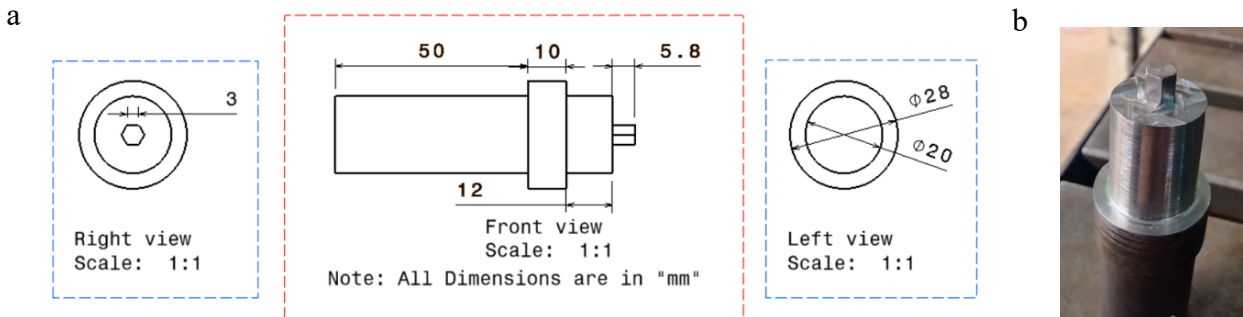


Fig. 3 Tool pin profile (a) Tool dimensions; (b) H13 hexagonal pin profile

Table 2 List of process variables

Factors	Setting 1	Setting 2	Setting 3
TRS (<i>rpm</i>)	900	1120	1400
WS (<i>mm/min</i>)	20	40	60
TTA (°)	0	1	2

2.2 Design of Experiment

The full factorial design approach is used to arrange the operations. In these three levels and three factors, the rotating speed was regulated at three levels: 900, 1120, and 1400 rpm, the WS at 20, 40, and 60 mm/min, and the TTA at 0, 1, 2°. To get Taguchi's L27 orthogonal array, the experiment was performed three times for each welding setting that used a total of 27 produced specimens. Table 3 depicts the experimental design for Taguchi L27 OA. The obtained data were statistically processed with Minitab software, and a Signal-to-Noise ratio ANOVA performed to assess main effects. The mean response difference, this shows that an independent variable affects the dependent variable, was used to determine the main effects (UTS). The UTS of welded samples was estimated using ASTM E8M-04 standard. The universal testing device (FIE Make Universal Testing Machine, UTES 40 HGFL) was employed for the tensile test. The measurements of the dog bone specimen as per the standard are shown in Fig. 5.

a

b

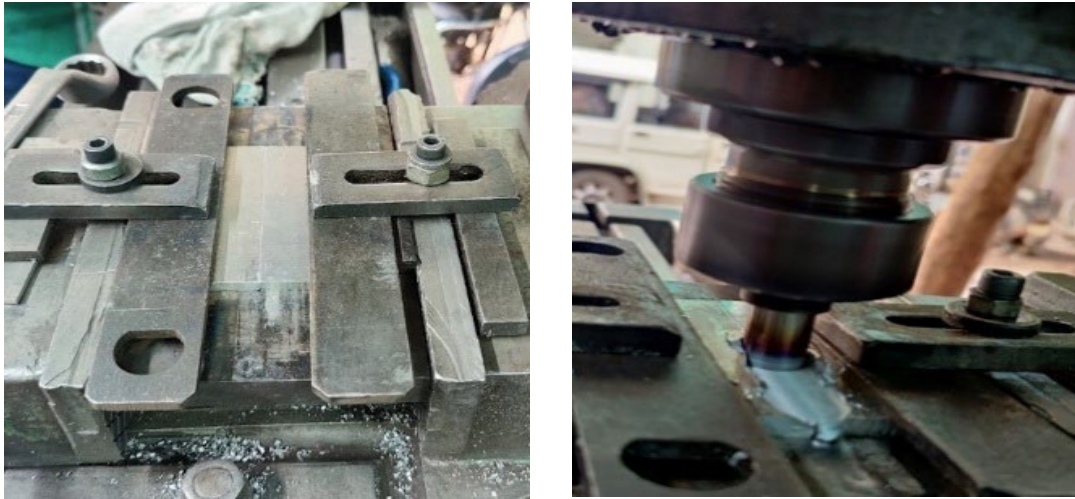


Fig. 4 (a) Plate clamping in fixtures; (b) FSW joining operation of dissimilar materials

Table 3 - Experimental design for the Taguchi L27 OA

S.No.	TRS (rpm)	WS (mm/min)	TTA (°)
1	900	20	0
2	900	20	0
3	900	20	0
4	900	40	1
5	900	40	1
6	900	40	1
7	900	60	2
8	900	60	2
9	900	60	2
10	1120	20	1
11	1120	20	1
12	1120	20	1
13	1120	40	2
14	1120	40	2
15	1120	40	2
16	1120	60	0
17	1120	60	0
18	1120	60	0
19	1400	20	2
20	1400	20	2
21	1400	20	2
22	1400	40	0
23	1400	40	0
24	1400	40	0
25	1400	60	1
26	1400	60	1
27	1400	60	1

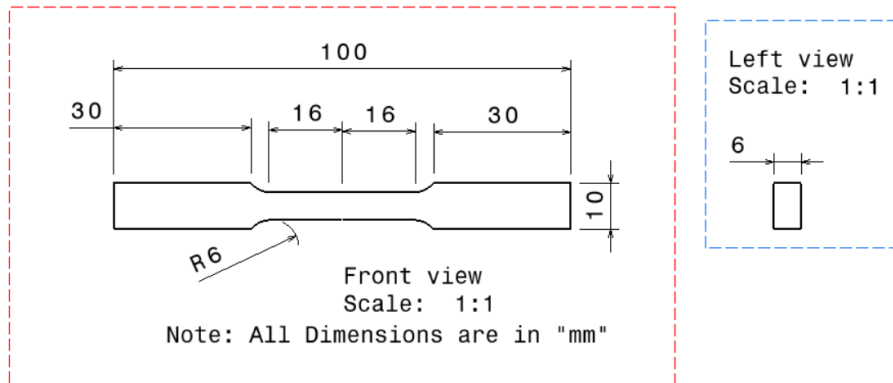


Fig. 5 Dimensions of a dog bone specimen

2.3 Machine Learning Algorithm

A regression model based on Random Forest Regression and Artificial Neural Networks was applied for forecasting strength of friction stir welded plates. Graph analysis and model performance are used to develop models in the next step. There are two sets of experimental results, one containing training data and the other containing test data. The training dataset is composed of 80% of the data from 27 observations, while the test dataset is composed of the remaining 20%. ANN and random forest regression models are constructed using machine learning algorithms. Next, developed models are tested on test data to determine their adequacy based on model performance and graph analysis.

Random Forest Regression Model: To achieve more reliable and accurate results, this approach creates a forest by combining different tree predictor combinations. Input nodes are generated separately for each tree. Classification and regression difficulties can be solved using this method. An example of a random forest approach schematic design for 27 trees is shown in Fig. 6. Instead of picking one solution during node splitting, this strategy chooses the best solution among numerous sub-solutions. The model introduced by this technique is more random than those created by other machine learning techniques [23]. Most of the models generated by the procedure are superior. A random variable is chosen at each node for the tree's growth. It is possible to obtain multiple outcomes from a single input using this machine learning approach. To improve the reliability of the approach, the average output is used for prediction outcomes [24].

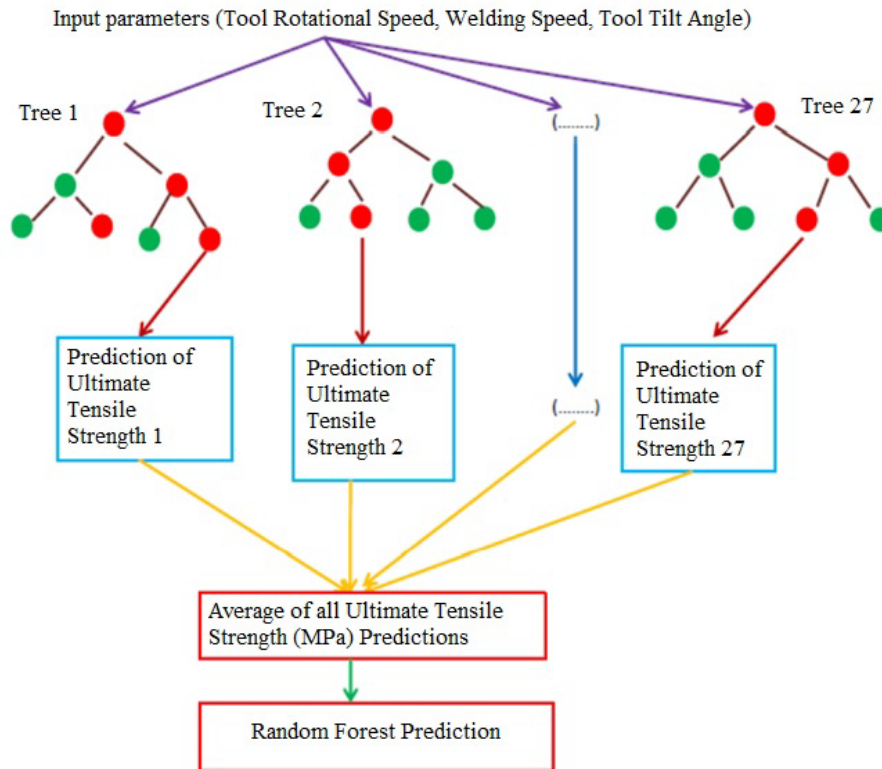


Fig. 6 Random forest algorithm [9]

Artificial Neural Networks: A biological neuron system is composed of neurons that learn through experience, and this tool is commonly used in data processing for prediction and categorization. There are several features of the method that make it appealing for tackling option pricing problems which do not rely on restrictive assumptions implied by parametric approaches or the specified theory of the relationship between asset and option prices. It is considered successful when an ANN can apply learning to new data after learning from the data [13]. Table 4 represents the hyperparameter of ANN.

Table 4 Hyperparameter selection for algorithm implementation

ML algorithm	Hyperparameter
RFR	Number of trees in the forest =27 Minimum sample split = 2 Minimum sample leaf = 1 n_estimator = 100 maximum depth =20
ANN	activation='relu' optimizer='adam' epochs=2000

3. Results and Discussion

3.1 Estimating UTS

Table 5 depicts tensile test results of both alloys. indicate that failure occurred inside the weld area. UTS of 190.21 MPa was attained at 1120 rpm TRS, 1° TTA & 20 mm/min WS. Using 900 rpm TRS, 2° TTA & 60 mm/min WS, lowest tensile strength of 131.20 MPa was reached.

Table 5 Tensile test results of AA5803/AA6082 FSW samples

S.No.	TRS (rpm)	WS (mm/min)	TTA (°)	UTS (MPa)	Failure location
1	900	20	0	170.90	Sample broken inside the weld
2	900	20	0	160.66	Sample broken inside the weld
3	900	20	0	181.14	Sample broken inside the weld
4	900	40	1	155.67	Sample broken inside the weld
5	900	40	1	160.10	Sample broken inside the weld
6	900	40	1	157.67	Sample broken inside the weld
7	900	60	2	137.94	Sample broken inside the weld
8	900	60	2	139.30	Sample broken inside the weld
9	900	60	2	131.20	Sample broken inside the weld
10	1120	20	1	190.21	Sample broken inside the weld
11	1120	20	1	178.45	Sample broken inside the weld
12	1120	20	1	180.78	Sample broken inside the weld
13	1120	40	2	164.32	Sample broken inside the weld
14	1120	40	2	174.14	Sample broken inside the weld
15	1120	40	2	183.93	Sample broken inside the weld
16	1120	60	0	165.07	Sample broken inside the weld
17	1120	60	0	160.96	Sample broken inside the weld
18	1120	60	0	149.18	Sample broken inside the weld
19	1400	20	2	164.79	Sample broken inside the weld
20	1400	20	2	176.64	Sample broken inside the weld
21	1400	20	2	152.94	Sample broken inside the weld
22	1400	40	0	160.40	Sample broken inside the weld
23	1400	40	0	163.97	Sample broken inside the weld
24	1400	40	0	167.53	Sample broken inside the weld
25	1400	60	1	143.26	Sample broken inside the weld
26	1400	60	1	148.18	Sample broken inside the weld
27	1400	60	1	153.10	Sample broken inside the weld

In Fig. 7, flux was observed around the aluminium plate during welding. The friction pressure mainly affects flash formation, causing the aluminium side to be significantly deformed [25], resulting in more intense flash effect because of the increased axial loads [26]. Tensile tests were performed on the specimens after they had undergone the FSW process. Fig. 8 illustrates a processed welded joint and wire cut tensile specimen and fractured tensile test specimen. Fig. 8 (c) represents the fracture location of all 27 tensile specimens.



Fig. 7 Flash generation during FS welding on the aluminium alloy plates

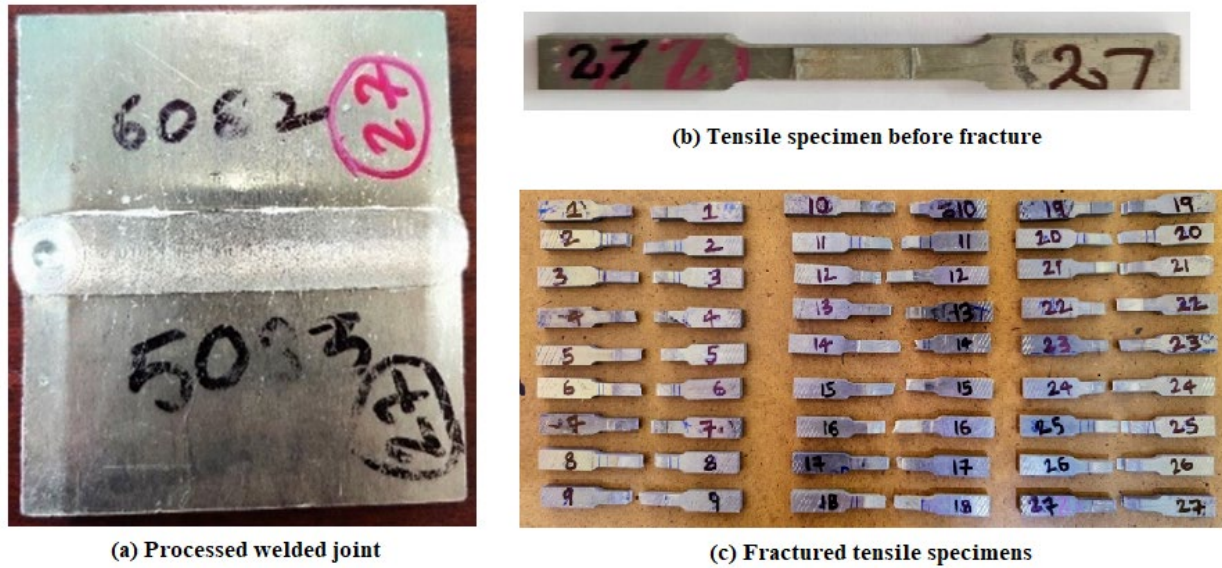


Fig. 8 Welded joint specimen

3.2 Statistical Analysis

Taguchi L27 orthogonal approach was used for FSW of AA5083 & AA6082. Below are graphs of the optimal parameter and S/N ratio plots. Tensile strength measured is presented in Tables 6 & 7 whereas S/N and mean effect plots are exhibited in Fig. 9. By using equation 1, the most optimal parameters for friction stir welds AA5083 and AA6082 (the larger the ratio, the better) are determined using MINITAB software. Generally, the higher the signal-to-noise ratio, the stronger the connection between WS, TRS, and TTA.

$$\frac{S}{N} = -10 \log \left(\sum \frac{\left(\frac{1}{y^2} \right)}{n} \right) \quad (1)$$

where 'y' indicates trial result and 'n' number of trials.

Table 6 S/N ratio analysis on tensile strength responses of AA alloys

Level	TRS (rpm)	WS (mm/min)	TTA (°)
1	43.75	44.72	44.30
2	44.67	44.35	44.21
3	44.00	43.35	43.92
Delta	0.92	1.37	0.38
Rank	2	1	3

Table 7 Mean analysis on tensile strength responses of AA alloys

Level	TRS (rpm)	WS (mm/min)	TTA (°)
1	155.0	172.9	164.4
2	171.9	165.3	163.1
3	159.0	147.6	158.4
Delta	16.9	25.4	6.1
Rank	2	1	3

By using Taguchi S/N - "Larger is better" condition, the optimal parameters for AA6082/AA5083 friction stir welds are determined using MINITAB21 as displayed in Table 8.

Table 8 Optimum process variable for UTS

	TRS (rpm)	WS (mm/min)	TTA (°)
Ultimate tensile strength	1120	20	1

As shown in Fig. 9 (a) & (b), these operating process parameters greatly influence the performance measure. This also has a significant effect on UTS, as indicated by the deviation of the response line from the horizontal line. AA 5083/6082 material is machined with the H13 tool using WS and TRS as the prominent input variables and TTA as least significant. 190.21 MPa tensile strength was achieved at 1120 rpm, 20 mm/min, and 1° when the tool rotated at 1120 rpm. At 900 rpm, 60 mm/min, and 2°, the tool exhibited the lowest UTS of 131.20 MPa.

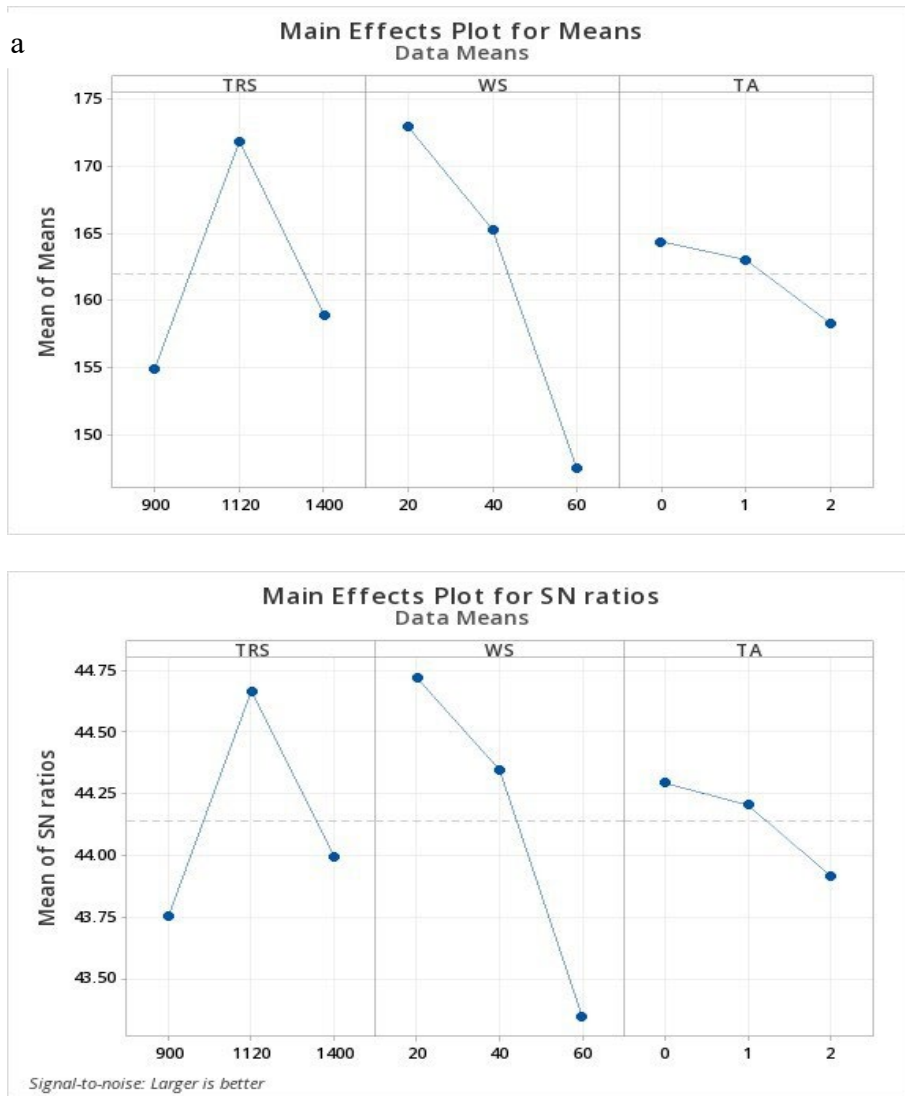


Fig. 9 Main effect plots (a) SN ratio; (b) Means

3.3 ANOVA for UTS

In ANOVA, it is possible to identify the process parameters that have the most influence on performance characteristics. Table 9 exhibits ANOVA on UTS results. According to Table 10, WS has a significant influence on UTS, followed by TRS and TTA. UTS was increased by 64.42 % by WS, 28.88 % by TRS, and 4.96 % by TTA as shown in Table 10.

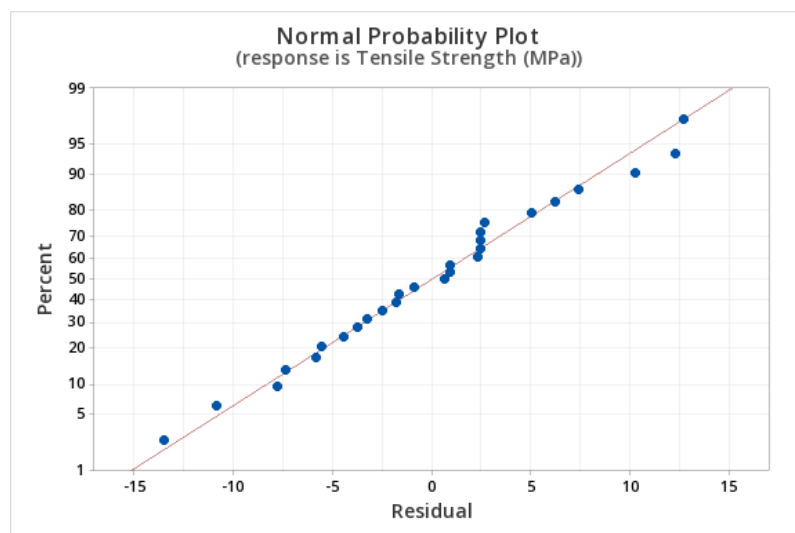
Table 9 ANOVA for UTS

Sources	DOF	Sum of squares	Mean square	% contribution
TRS	2	1.35270	0.67635	28.88 %
WS	2	3.01690	1.50845	64.42%
TTA	2	0.23235	0.11617	4.96%
Residual Error	2	0.08076	0.04038	
Total	8	4.68272		

Modeling: Statistical models have been developed to predict UTS with TRS, weld speed, and TTA using linear regression analysis in the Minitab software tool. No transformations have been applied to the responses. Equation (2) shows the predictive equation derived from the regression analysis for UTS.

$$\begin{aligned} \text{Tensile Strength(MPA)} = & 161.94 - 6.99 \text{ TRS}_{900} + 9.95 \text{ TRS}_{1120} - \\ & 2.96 \text{ TRS}_{1400} + 11.00 \text{ WS}_{20} + 3.36 \text{ WS}_{40} - \\ & 14.37 \text{ WS}_{60} + 2.48 \text{ TTA}_0 + 1.10 \text{ TTA}_1 - 3.59 \text{ TTA}_2 \quad R^2 = 80.81\% \end{aligned} \quad (2)$$

A regression model developed for UTS had an R^2 value of 80.81% in the present study. For evaluating the significance of the coefficients, a residual plot was used. In the case of a straight residual plot, it means that the residual errors are normally distributed, and the coefficients are significant. In Fig. 10, the residual values for UTS are approximating a straight-line indicating development of significant coefficients.

**Fig. 10** Residuals normal probability plot for UTS

3.4 Machine Learning Evaluation

The input variables for data sets are TRS, WS, and TTA whereas the output variable is UTS. To calculate performance parameters, MAE, RMSE, R^2 , and MSE values are used. Training and testing datasets employed are exhibited in Tables 10 and 11 respectively. Evaluation of the model's response is based on its performance characteristics (MAE, MSE, and RMSE, R^2). The UTS of the FSW process is determined using ANN and random forest regression techniques. Table 11 shows the parameters used for evaluating the performance of random forest regressions. UTS's actual value and its predicted value are demonstrated in Fig.11 and Fig. 12. Fig. 11 exhibits training data set and Fig. 12 shows test data set. According to the experimental results, training data and test data are consistent. In the present study, RFR and ANN techniques are considered for modeling the nonlinear correlation between output and input parameters. Table 12 shows the R^2 score, MAE, MSE, and RMSE values. Training and test data results were akin to those from experimentation. Thus, RFR is an effective method to model nonlinear relationship among input and output variables. RFR has an R^2 of 0.90 and ANN has an R^2 of 0.87, which is not bad. An R^2 value of 1 means the model is accurate, while a value of 0 means it does not perform well on unseen datasets. In addition, R^2 value of 1 indicates better model training. While RFR gives accurate results when

there is less data, ANN needs more data to produce precise results. RFR has a coefficient of determination of 0.90, which is higher than ANN's 0.87. It is observed that RFR has a minimum absolute error of 2.82. This graph illustrates the similarity between the prediction results of the random forest technique and those obtained using UTS experimentation. With the random forest regressor technique, predicted and actual UTS values follow the same trend. Fig. 13 shows how UTS varies with the number of test sets. The graph clearly demonstrates RFR predicted UTS values are comparable to the actuals. The plots indicate that with the random forest technique, predicted and real UTS values follow almost the same trend. Fig. 14 depicts residuals of predicted and experimental UTS values for the test dataset. Fig. 15 shows the error of experimental datasets for ANN and RFR of UTS values calculated for actual and predicting values.

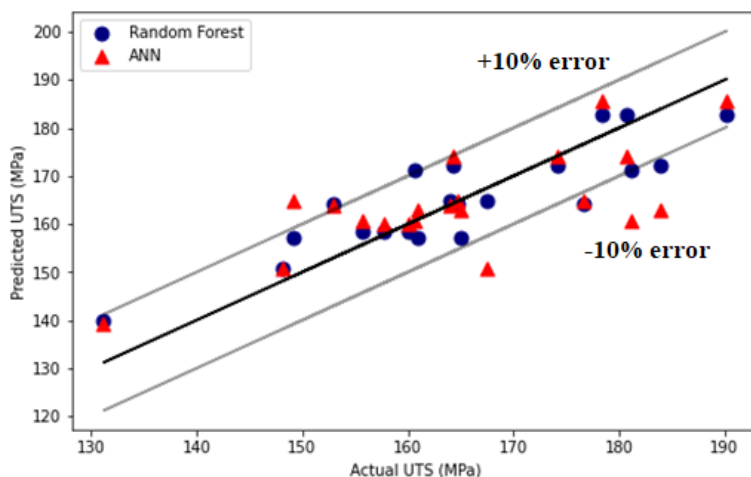


Fig. 11 Comparison of actual and predicted UTS based on training datasets

Table 10 UTS responses based on training datasets

S.No.	TRS (rpm)	WS (mm/min)	TTA (°)	Actual UTS values (MPa)	ANN predicted UTS values (MPa)	RFR predicted UTS values (MPa)
1	900	20	0	160.66	160.663	171.2
2	900	20	0	181.14	160.663	171.2
3	900	20	0	155.67	160.663	158.4
4	900	40	1	160.1	160.1	158.4
5	900	40	1	157.67	160.1	158.4
6	900	60	2	131.2	139.303	139.88
7	1120	20	1	190.21	185.491	182.82
8	1120	20	1	178.45	185.491	182.82
9	1120	40	2	180.78	174.127	182.82
10	1120	40	2	164.32	174.127	172.34
11	1120	40	2	174.14	174.127	172.34
12	1120	60	0	183.93	163.015	172.34
13	1120	60	0	165.07	163.015	157.11
14	1120	60	0	160.96	163.015	157.11
15	1400	20	2	149.18	164.792	157.11
16	1400	20	2	164.79	164.792	164.1
17	1400	20	2	176.64	164.792	164.1
18	1400	40	0	152.94	163.969	164.1
19	1400	40	0	163.97	163.969	164.72
20	1400	60	1	167.53	150.64	164.72

21 1400 60 1 148.18 150.64 150.7

Table 11 UTS responses based on test data

S.No.	TRS (rpm)	WS (mm/min)	TTA (°)	Actual UTS values (MPa)	ANN predicted UTS values (MPa)	RFR predicted UTS values (MPa)
1	900	40	1	170.90	160.059	171.2
2	900	60	2	137.94	139.315	139.878
3	900	60	2	139.30	139.315	139.878
4	1120	20	1	160.40	185.485	164.715
5	1400	40	0	143.26	150.639	150.698
6	1400	60	1	153.10	163.968	164.715

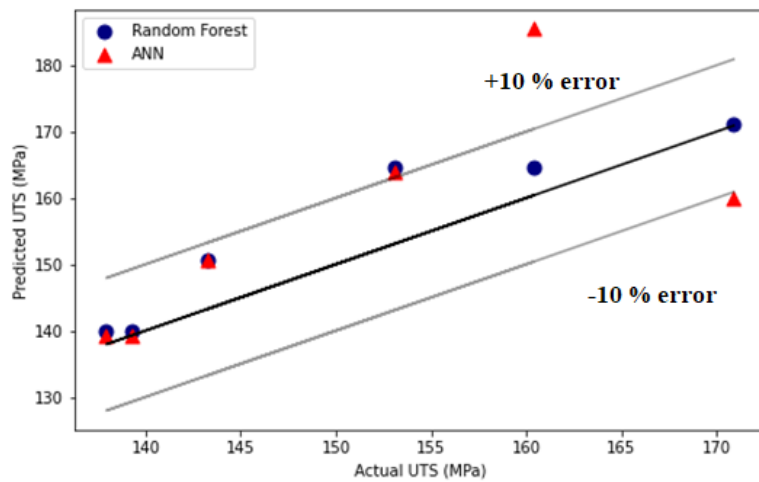


Fig. 12 Actual vs. predicted UTS (test data)

Table 12 Values of R2, MAE, MSE, RMSE

	R ² score	MAE	MSE	RMSE
Random forest regression	0.90	2.82	13.98	3.73
ANN	0.87	4.98	3.51	5.52

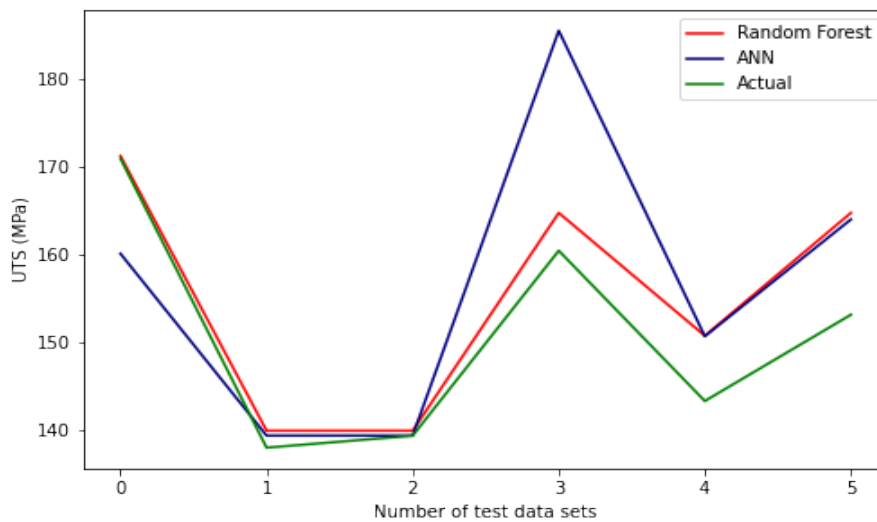


Fig. 13 Variation of UTS (MPa) relative to test datasets

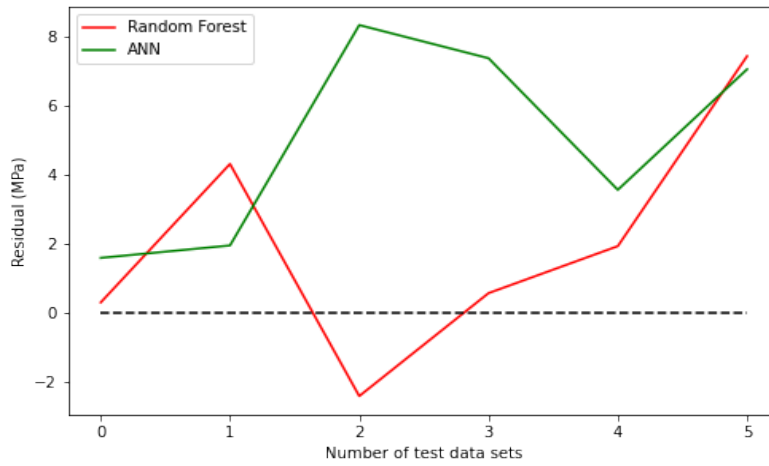
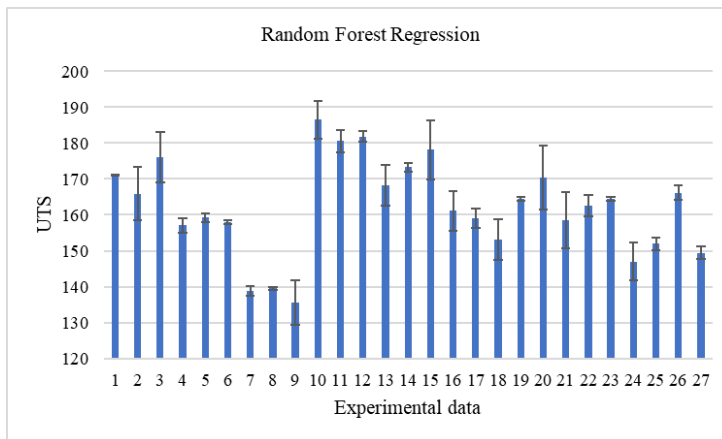
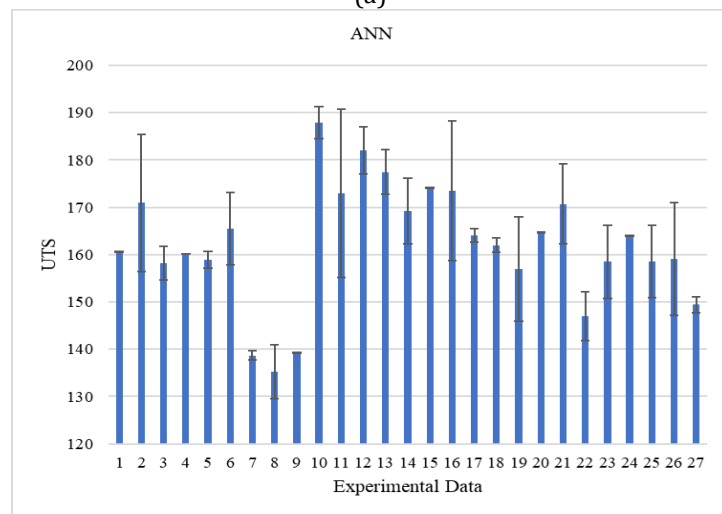


Fig. 14 Variation of residual (MPa) relative to test datasets



(a)



(b)

Fig. 15 Error graphs for the experimental data (a) Random forest regression; (b) ANN

4. Feature Importance Analysis

Feature significance is employed in identifying the most influential input variable that contributes to the output. Fig. 16 portrays results of feature importance analysis wherein welding speed is the prime variable for predicting

the UTS. In terms of predictivity, TTA angle ($^{\circ}$) represents less than 5 %, TRS represents around 29%, and WS is the most significant parameter, with a score of more than 64%. Altering weld speed generally impacts weld quality. On the basis of feature importance test, Pareto chart of standardized effects confirmed welding speed as a significant variable in predicting UTS. Increase of weld speed enhances the scale of force conveyed on FSW tool. The higher the weld speed, lower is the frictional heat with pronounced endurance of material to the tool motion [27]. This conforms to the results already reported in the literature that welding speed is critical in determining weld length based frictional heat exposure duration. Consequently, grain development and precipitates inside the fused material are affected. Obtaining an ideal exposure period and suitable translation of agitated material results in successful material consolidation. It is also noted that the output is not influenced by rotational speed (RPM) [28-29]. Fig. 17 shows relative comparison of loss function using training and test datasets. Loss value is anticipated to be low with the increase of epochs. A 2000 epoch training dataset was employed for training, and as envisaged the loss decreased with more epochs. As the number of training epochs increases, the MSE decreases. It is also possible to overfit the training data when increases occur as well. Loss function is validated using the test dataset which exhibited consonance with the loss profile based on training dataset. The best validation performance (MSE) at epoch 1088 was 0.0616. Overall accuracy of the NN model was found to be 87.196%. As seen from the graph plot on training loss, validation loss and accuracy accomplished, the NN model seems to be a fit model.

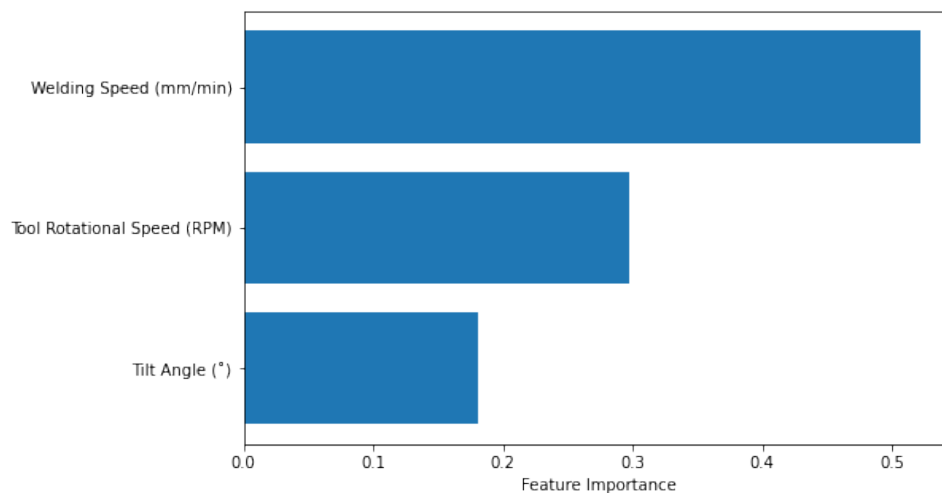


Fig. 16 Feature importance analysis of process parameters

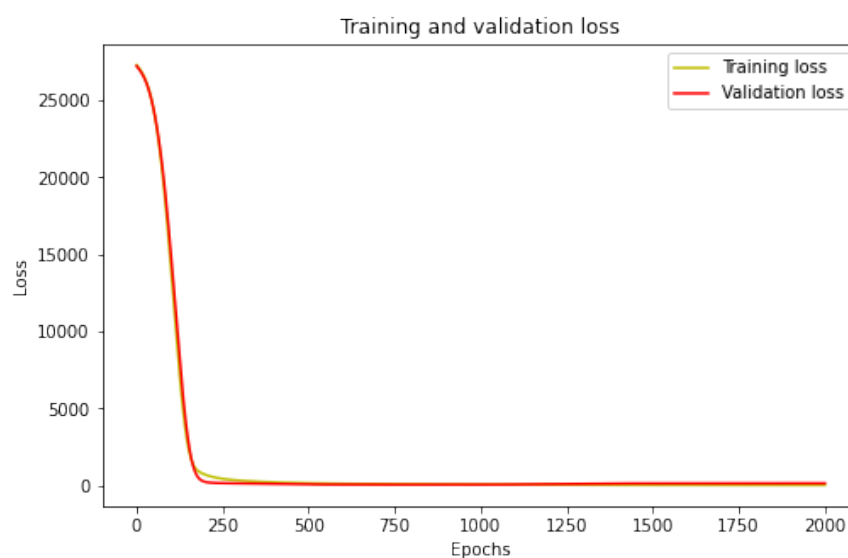


Fig. 17 Plot of the loss function concerning epochs

5. Conclusions

In this study, RFR and ANN techniques are explored in the manufacturing field. AA5083/AA6082 FSW joints with dissimilar materials are estimated using two regression models. Relative comparison of both the regression models was made for determining the best regression model. These techniques can be applied to analyze joint quality of FSW AA plates based on current findings. S/N ANOVA is also used to check the results. According to the ANOVA, all models predict UTS values significantly. Additionally, the RFR technique (R^2 0.90, RMSE 3.73 MPa) performs better than the ANN (R^2 0.87, RMSE 5.52 MPa) for the present dataset. Compared to other process parameters, WS was the most significant factor.

Acknowledgement

The authors fully acknowledged VNR Vignana Jyothi Institute of Engineering and Technology for supporting this work.

Conflict of Interest

Authors declare that there is no conflict of interests regarding the publication of the paper.

References

- [1] DebRoy, T., & Bhadeshia, H. K. D. H. (2010). Friction stir welding of dissimilar alloys—a perspective. *Science and Technology of Welding and Joining*, 15(4), 266-270. <https://doi.org/10.1179/174329310X12726496072400>
- [2] Kasman, S., Kahraman, F., Emiralioğlu, A., & Kahraman, H. (2017). A case study for the welding of dissimilar EN AW 6082 and EN AW 5083 aluminum alloys by friction stir welding. *Metals*, 7(1), 6. <https://doi.org/10.3390/met7010006>
- [3] Vimalraj, C., & Kah, P. (2021). Experimental review on friction stir welding of aluminium alloys with nanoparticles. *Metals*, 11(3), 390. <https://doi.org/10.3390/met11030390>
- [4] Threadgill, P. L., Leonard, A. J., Shercliff, H. R., & Withers, P. J. (2009). Friction stir welding of aluminium alloys. *International Materials Reviews*, 54(2), 49-93. <https://doi.org/10.1179/174328009X411136>
- [5] Sudhagar, S., Sakthivel, M., & Ganeshkumar, P. (2019). Monitoring of friction stir welding based on vision system coupled with machine learning algorithm. *Measurement*, 144, 135-143. <https://doi.org/10.1016/j.measurement.2019.05.018>
- [6] Verma, S., Misra, J. P., & Popli, D. (2022). Modeling of friction stir welding of aviation grade aluminium alloy using machine learning approaches. *International Journal of Modelling and Simulation*, 42(1), 1-8. <https://doi.org/10.1080/02286203.2020.1803605>
- [7] Verma, S., Gupta, M., & Misra, J. P. (2018). Performance evaluation of friction stir welding using machine learning approaches. *MethodsX*, 5, 1048-1058. <https://doi.org/10.1016/j.mex.2018.09.002>
- [8] Mishra, A., Sefene, E. M., & Tsegaw, A. A. (2021). Process parameter optimization of friction stir welding on 6061AA using supervised machine learning regression-based algorithms. *arXiv preprint arXiv:2109.00570*. <https://doi.org/10.48550/arXiv.2109.00570>
- [9] Mishra, A. (2020). Artificial intelligence algorithms for the analysis of mechanical property of friction stir welded joints by using python programming. *Welding Technology Review*, 92(6), 7-16. <https://doi.org/10.26628/wtr.v92i6.1120>
- [10] Elatharasan, G., & Kumar, V. S. (2013). An experimental analysis and optimization of process parameter on friction stir welding of AA 6061-T6 aluminum alloy using RSM. *Procedia Engineering*, 64, 1227-1234. <https://doi.org/10.1016/j.proeng.2013.09.202>
- [11] Eren, B., Guvenc, M. A., & Mistikoglu, S. (2021). Artificial intelligence applications for friction stir welding: a review. *Metals and Materials International*, 27, 193-219. <https://doi.org/10.1007/s12540-020-00854-y>
- [12] Nasir, T., Asmaela, M., Zeeshana, Q., & Solyalib, D. (2020). Applications of machine learning to friction stir welding process optimization. *Jurnal Kejuruteraan*, 32(2), 171-186. [https://doi.org/10.17576/jkukm-2020-32\(2\)-01](https://doi.org/10.17576/jkukm-2020-32(2)-01)
- [13] Balachandar, K., Jegadeeshwaran, R., & Gandhikumar, D. (2020). Condition monitoring of FSW tool using vibration analysis—a machine learning approach. *Materials Today: Proceedings*, 27, 2970-2974. <https://doi.org/10.1016/j.matpr.2020.04.903>
- [14] Vignesh, R. V., & Padmanaban, R. (2018). Artificial neural network model for predicting the tensile strength of friction stir welded aluminium alloy AA1100. *Materials Today: Proceedings*, 5(8), 16716-16723. <https://doi.org/10.1016/j.matpr.2018.06.035>
- [15] Mishra, A. (2020). Machine learning algorithm for surface quality analysis of friction stir welded joint. *Strojnícky Časopis-Journal of Mechanical Engineering*, 70(2), 11-20. <https://doi.org/10.2478/scjme-2020-0016>
- [16] Mishra, A. (2020). Understanding machine learning for friction stir welding technology. Available at SSRN: <https://ssrn.com/abstract=3560731>. <http://dx.doi.org/10.2139/ssrn.3560731>

- [17] Verma, S., Misra, J. P., Singh, J., Batra, U., & Kumar, Y. (2021). Prediction of tensile behavior of FS welded AA7039 using machine learning. *Materials Today Communications*, 26, 101933. <https://doi.org/10.1016/j.mtcomm.2020.101933>
- [18] Mishra, A. (2020). Machine learning approach for defects identification in dissimilar friction stir welded aluminium alloys AA 7075-AA 1100 joints. *Journal of Aircraft and Spacecraft Technology*, 4(1), 88-95. <https://doi.org/10.3844/jastsp.2020.88.95>
- [19] Mishra, A. (2020). Machine learning classification models for detection of the fracture location in dissimilar friction stir welded joint. *Applied Engineering Letters: Journal of Engineering and Applied Sciences*, 5(3), 87-93. <https://doi.org/10.18485/aeletters.2020.5.3.3>
- [20] Darmadi, D. B., Mentary, A., Yusup, E. M., & Mahzan, S. (2019). Evaluating the effect of the pin's length to the strength of double sides friction stir welded aluminum. *International Journal of Integrated Engineering*, 11(5), 1-11. <https://doi.org/10.30880/ijie.2019.11.05.001>
- [21] Abd El-Hafez, H., & El-Megharbel, A. (2018). Friction stir welding of dissimilar aluminum alloys. *World Journal of Engineering and Technology*, 6, 408-419. <https://doi.org/10.4236/wjet.2018.62025>
- [22] Mullaierasu, R., Thilagham, K. T., & Noorullah, D. (2021). A study of the optimization and characterization of friction stir welded AA5083 and AA6082. *International Research Journal on Advanced Science Hub*, 3(6), 131-139. <http://dx.doi.org/10.47392/irjash.2021.152>
- [23] Rodriguez-Galiano, V. F., Ghimire, B., Rogan, J., Chica-Olmo, M., & Rigol-Sanchez, J. P. (2012). An assessment of the effectiveness of a random forest classifier for land-cover classification. *ISPRS Journal of Photogrammetry and Remote Sensing*, 67, 93-104. <https://doi.org/10.1016/j.isprsjprs.2011.11.002>
- [24] Quinlan, J. R. (1992). Learning with continuous classes. *Proceedings AI'92*, World Scientific, 92, 343-348. <https://sci2s.ugr.es/keel/pdf/algorithm/congreso/1992-Quinlan-AI.pdf>
- [25] Liu, Y., Zhao, H., Peng, Y., & Ma, X. (2019). Microstructure characterization and mechanical properties of the continuous-drive axial friction welded aluminum/stainless steel joint. *International Journal of Advanced Manufacturing Technology*, 104, 4399-4408. <https://doi.org/10.1007/s00170-019-04245-5>
- [26] Taban, E., Gould, J. E., & Lippold, J. C. (2010). Dissimilar friction welding of 6061-T6 aluminum and AISI 1018 steel: properties and microstructural characterization. *Materials & Design*, 31(5), 2305-2311. <https://doi.org/10.1016/j.matdes.2009.12.010>
- [27] Vivas, J., Fernández-Calvo, A. I., Aldanondo, E., Irastorza, U., & Álvarez, P. (2022). Friction stir weldability at high welding speed of two structural high pressure die casting aluminum alloys. *Journal of Manufacturing and Materials Processing*, 6(6), 160. <https://doi.org/10.3390/jmmp6060160>
- [28] Mishra, A., & Dasgupta, A. (2022). Supervised and unsupervised machine learning algorithms for forecasting the fracture location in dissimilar friction-stir-welded joints. *Forecasting*, 4(4), 787-797. <https://doi.org/10.3390/forecast4040043>
- [29] Di Bella, G., Favaloro, F., & Borsellino, C. (2023). Effect of process parameters on friction stir welded joints between dissimilar aluminum alloys: a review. *Metals*, 13(7), 1176. <https://doi.org/10.3390/met13071176>